Neuropsychologia 60 (2014) 131–143

Contents lists available at ScienceDirect

Neuropsychologia

journal homepage: www.elsevier.com/locate/neuropsychologia

Parcellation of left parietal tool representations by functional connectivity

Frank E. Garcea [a,b], Bradford Z. Mahon [a,b,c,*]

[a] Department of Brain and Cognitive Sciences, University of Rochester, USA
[b] Center for Visual Science, University of Rochester, USA
[c] Department of Neurosurgery, University of Rochester, USA

ARTICLE INFO

Article history:
Received 12 December 2013
Received in revised form
30 April 2014
Accepted 26 May 2014
Available online 2 June 2014

Keywords:
Parietal cortex
Manipulable objects
Functional connectivity
fMRI
Apraxia

ABSTRACT

Manipulating a tool according to its function requires the integration of visual, conceptual, and motor information, a process subserved in part by left parietal cortex. How these different types of information are integrated and how their integration is reflected in neural responses in the parietal lobule remains an open question. Here, participants viewed images of tools and animals during functional magnetic resonance imaging (fMRI). *k*-Means clustering over time series data was used to parcellate left parietal cortex into subregions based on functional connectivity to a whole brain network of regions involved in tool processing. One cluster, in the inferior parietal cortex, expressed privileged functional connectivity to the left ventral premotor cortex. A second cluster, in the vicinity of the anterior intraparietal sulcus, expressed privileged functional connectivity with the left medial fusiform gyrus. A third cluster in the superior parietal lobe expressed privileged functional connectivity with dorsal occipital cortex. Control analyses using Monte Carlo style permutation tests demonstrated that the clustering solutions were outside the range of what would be observed based on chance 'lumpiness' in random data, or mere anatomical proximity. Finally, hierarchical clustering analyses were used to formally relate the resulting parcellation scheme of left parietal tool representations to previous work that has parcellated the left parietal lobule on purely anatomical grounds. These findings demonstrate significant heterogeneity in the functional organization of manipulable object representations in left parietal cortex, and outline a framework that generates novel predictions about the causes of some forms of upper limb apraxia.

1. Introduction

1.1. Manipulable object knowledge

The ability to use objects according to their function and in the correct context requires the integration of diverse types of information. Consider, for instance, the knowledge and skills involved in the everyday action of picking up a fork and eating some food off of your plate. The target of the initial reaching action must be identified, and a reach-to-grasp action planned and executed. That reach-to-grasp action is based on a prior identification of the particular fork, which is the target of the action (e.g., your fork as opposed to your neighbor's fork). The reaching action must then take into account various obstacles that may be present (e.g., a glass of wine, your neighbor's elbow). Furthermore, the reach-to-grasp action ultimately anticipates the way in which the object (fork) will be manipulated, and as such, depends on the integration of identity information and knowledge of the center of mass of that object. For instance, different forks will be picked up at different points along the handle according to their center of mass, but a fork and knife with the same center of mass will also be picked up differently, according to the eventual way the object will be held for use. Then, once the fork is 'in hand,' the way in which it is manipulated depends on an understanding of how forks work—you don't use it to scoop a piece of steak that could be stabbed, and you don't use it to stab your mashed potatoes but instead scoop them.

When unpacked in this way, it becomes clear that even a simple action like reaching out to pick up a fork to eat dinner is a complex process that requires the integration of many different types of information. A range of previous research has demonstrated the involvement of temporal, parietal, occipital and frontal cortex—that is, a whole brain network—in tool processing. For instance, viewing manipulable objects compared to comparable baseline categories (animals, vehicles) leads to differential neural responses in regions of the inferior and superior parietal lobule, ventral and lateral temporo-occipital regions, dorsal occipital cortex, and premotor cortex (e.g., Chao, Haxby, & Martin, 1999;

* Correspondence to: University of Rochester, Meliora Hall, Rochester, NY 14627-0268, USA. Tel.: +1 585 276 5234; fax: +1 585 276 2127.
E-mail address: mahon@rcbi.rochester.edu (B.Z. Mahon).

http://dx.doi.org/10.1016/j.neuropsychologia.2014.05.018
0028-3932/

Chao & Martin, 2000; Fang & He, 2005; Mahon et al., 2007; Mahon, Kumar, & Almeida, 2013; Martin, Wiggs, Ungerleider, & Haxby, 1996; Nopponey, Price, Penny, & Friston, 2006; Rumiati et al., 2004; for review, see Lewis, 2006). These regions are generally left lateralized, with the exception of the superior/posterior parietal cortex and the fusiform gyrus. We refer to this entire network of regions, which is implicated in the recognition and use of manipulable objects, as the Tool Processing Network.

Different regions within the Tool Processing Network carry out different aspects of the complex process of object-directed action. For instance, ventral temporal-occipital regions represent visual, visuo-semantic and surface texture information about objects (e.g., see Campanella, D'Agostini, Skrap, & Shallice, 2010; Cant & Goodale, 2011; Capitani, Laiacona, Mahon, & Caramazza, 2003; Gainotti, 1995, 2000; Miceli, Fouch, Capasso, Shelton, Tomaiuolo, & Caramazza, 2001; Rogers, Hocking, Mechelli, Patterson, & Price, 2005). Lateral temporal cortex, in the vicinity of the left posterior middle temporal gyrus and the inferior temporal gyrus, is particularly responsive to the mechanical motion associated with tools (Beauchamp, Lee, Haxby, & Martin, 2002, 2003), and is anterior and ventral to motion area MT/V5. The left ventral premotor cortex is also involved in processing tool knowledge, and is thought to be important for action planning and sequencing (Chao & Martin, 2000; Grafton, Fadiga, Arbib, & Rizzolatti, 1997; Passingham, 1985). While the dorsal aspect of premotor cortex has also been associated with the processing of tools (e.g., Grafton et al., 1997), it is typically ventral and not dorsal premotor cortex that is activated during passive viewing of tools or tool naming (cf., Chao & Martin, 2000; Martin et al., 1996).

1.2. The role of left parietal cortex in tool use

It has been known since the pioneering work of Liepmann (1905) that the left parietal lobule plays a particularly central role in supporting complex object directed action. The activation elicited by tool stimuli in the left parietal lobule typically extends in one contiguous cluster from lateral and inferior regions (supramarginal gyrus) dorsally and posteriorly to include the anterior aspect of the IPS, and then caudally along the IPS to dorsal occipital cortex. While there are generally no tool-specific responses in the angular gyrus of the inferior parietal lobule (for review, see Lewis, 2006; Martin, 2007), there is evidence that the angular gyrus may be involved in the grasping phase of tool use (e.g., see Creem-Regehr & Lee, 2005; Johnson-Frey, Newman-Norlund, & Grafton, 2005).

There is already good evidence from neuropsychology to suggest a coarse parcellation of left parietal tool representations. A deficit in visually-guided reaching in peripersonal space is classically associated with damage to superior/posterior parietal cortex, and/or dorsal occipital cortex (Desmurget & Sirigu, 2009; Jeannerod, Arbib, Rizzolatti, & Sakata, 1995; Jeannerod, Decety, & Michel, 1994; Karnath & Perenin, 2005; Pisella et al., 2000), and functional neuroimaging studies designed to highlight the reach-to-grasp component of actions have found activation in posterior regions of parietal cortex (Cavina-Pratesi, Goodale, & Culham 2007; Culham et al., 2003; Konen, Mruczek, Montoya, & Kastner, 2013). In contrast, lesions to the anterior intraparietal sulcus (aIPS) tend to disrupt grip scaling of the fingers during reaching but may not affect the reach component of the action itself (Binkofski et al., 1999a, 1999b). Finally, limb apraxia, a deficit in performing skilled action, is classically associated with damage to the supramarginal gyrus of the left inferior parietal lobule (Liepmann, 1905). Patients with limb apraxia can be impaired for gesturing object use from verbal command, pantomiming object use from visual presentation of an object, and imitating actions (see, e.g., Buxbaum & Saffran, 2002; Buxbaum, Veramonti, & Schwartz, 2000; Garcea, Dombovy, & Mahon, 2013; Liepmann, 1905; Negri et al., 2007; Ochipa, Rothi, & Heilman, 1989; Rumiati, Zanini, Vorano, & Shallice, 2001; for reviews, see Binkofski & Buxbaum, 2013; Cubelli, Marchetti, Boscolo, & Della Sala, 2000; Goldenberg, 2009; Johnson-Frey, 2004; Leiguarda & Marsden, 2000; Mahon & Caramazza, 2005; Osiurak, Jarry, & Le Gall, 2009; Rothi, Ochipa, & Heilman, 1991).

It is clear that the computations underlying reach-to-grasp actions are supported by the classically defined dorsal stream, and as such, are computed 'on the fly' on the basis of the current state of the world (Milner & Goodale, 2008). In other words, you don't (typically) reach to grasp a glass on the basis of where you know it is, but on the basis of where you perceive it to be at the moment that the grasp is planned. However, it is not at all clear that complex object-associated manipulations could, in principle, be supported by only a dorsal stream analysis of the visual input. This is because complex object-associated manipulations are not given by the visual input. For instance, the knowledge of how a pair of pliers is used once the object is in hand, is information that is stored. In their influential model of apraxia Rothi, Heilman and colleagues analogized those action representations to lexical representations of words (e.g., Rothi et al., 1991; see also Negri et al., 2007).

Thus, in principle, it should be possible to dissociate tool activation across inferior parietal regions (manipulation component of action) and superior parietal regions (reach-to-grasp component of action) according to whether the provenance of the information is the ventral or dorsal stream, respectively. One way to accomplish this is to capitalize on asymmetries in how different classes of retinal ganglion cells map onto the two visual pathways (see Merigan & Maunsell, 1993)—because the dorsal visual pathway is biased against direct inputs from parvocellular channels, stimulus information that is preferentially processed in parvocellular channels (e.g., color, high spatial frequencies) should not, by hypothesis, be analyzed through the dorsal pathway. Recent functional imaging work with healthy subjects has shown that when visual stimuli are titrated psychophysically so that their processing is biased toward parvocellular channels (hence away from a dorsal visual pathway), tool-stimuli continue to elicit differential activation only in *inferior* regions of left parietal cortex, but not in posterior/superior regions of left parietal cortex (Almeida, Fintzi, & Mahon, 2013; Mahon et al., 2013). Furthermore, those same left inferior parietal regions that are activated for stimuli that are titrated so as to not be visible by the dorsal visual pathway exhibit privileged functional connectivity to regions of the Tool Processing Network in the ventral stream, such as the left medial fusiform gyrus. The reverse dissociation has also been observed: Using continuous flash suppression, Fang and He (2005) showed that suppressed images of tools continue to activate posterior parietal and dorsal occipital regions, even though processing within the ventral stream for the same stimuli was entirely abolished (for behavioral work and discussion, see Almeida, Mahon, & Caramazza, 2010; Almeida, Mahon, Nakayama, & Caramazza, 2008).

Thus, there is already strong precedent regarding the whole brain neural network that broadly supports object directed action, as well as indications about how to parcellate tool representations in parietal cortex on functional grounds. A largely separate literature has sought to develop a parcellation scheme for left parietal cortex based on cytoarchitecture, anatomical connectivity, and the distribution of neurotransmitter receptors (Borra et al., 2008; Borra, Ichinohe, Sato, Tanifuji, & Rockland, 2010; Caspers et al., 2011, 2006, 2013; Mars et al., 2011; Orban, et al., 2006; Ruschel et al., in press; Rushworth, Behrens, & Johansen-Berg, 2006). Some approaches have explicitly sought to parcellate the inferior parietal lobule (Caspers et al., 2011, 2006,

2013; Ruschel et al., in press; Zhong & Rockland, 2003), or superior parietal lobule (Konen & Kastner, 2008; Zhang et al., 2014), or the entire parietal lobule (Durand, et al., 2007; Konen et al., 2013; Mars et al., 2011; Nelsen, et al., 2010; Rushworth et al., 2006).

The goal of the current study is to use functional connectivity to test how tool representations in left parietal cortex are organized, and then to bring our findings into register with the existing literature on parietal organization. We believe that this kind of investigation is important, for two reasons. First, left parietal cortex is involved in a wide range of neurocognitive functions, including attention, eye movements, numeracy, working memory, phonological processing, and semantic processing (Binder, Desai, Graves, & Conant, 2009; Cabeza, Ciaramelli, Olson, & Moscovitch, 2008; Cantlon, 2013; Cantlon et al., 2009; Corbetta, 1998; Corbetta & Shulman, 2002; Hickok, 2009; Hickok & Poeppel, 2004; Konen, Kleiser, Wittsack, Bremmer, & Seitz, 2004; Rizzolatti & Matelli, 2003; Thiebaut de Schotten, Dell'Acqua, Forkel, Simmons, & Vergani, 2011). Thus, understanding how the parcellation of tool representations in left parietal cortex may or may not align with other, independent, parcellation schemes for left parietal cortex could shed light on whether there is a common set of functions that underpins the role(s) of left parietal cortex in diverse domains of cognitive processes. Second, because the functional properties and structural connections of the subregions of the left inferior parietal lobule have been extensively documented, studying where parietal tool representations "fit" within various parcellation schemes has important consequences for understanding the causes of upper limb apraxia.

A subgoal of the current study was to test whether tool processing within the left posterior middle temporal gyrus is more similar, in terms of its connectivity profile to parietal cortex, to the ventral stream (left medial fusiform gyrus) or the dorsal stream (left dorsal occipital cortex). Previous work indicates that computations carried out by the left posterior middle temporal gyrus during tool processing have elements that could be tied to either the dorsal or ventral steam. For instance, the left posterior middle temporal gyrus is involved in the processing of lexical semantics (Martin, 2007), processing verbs whose actions denote motion (Bedny, Caramazza, Pascual-Leone, & Saxe, 2012), and processing motion of nonliving entities (e.g., see Beauchamp et al., 2002, 2003).

We parcellate left parietal tool representations according to functional connectivity with four other regions that comprise the Tool Processing Network: (i) left ventral premotor cortex, (ii) left dorsal occipital cortex, (iii) left medial fusiform gyrus, and (iv) left posterior middle temporal gyrus. *k*-Means clustering is used to delineate the clusters inherent in functional connectivity data, and parallel region-of-interest (ROI) based functional connectivity analyses are then used to interpret the functional significance of the identified clusters. Thus, for all analyses, the number of *k* clusters was set to three because we are interested in parcellating parietal cortex based on (i) inputs from the ventral stream (left medial fusiform gyrus, left posterior middle temporal gyrus), (ii) inputs from the dorsal stream (left dorsal occipital cortex), and (iii) outputs to the motor system (left premotor cortex).

2. Methods

2.1. Participants

The current investigation is a re-analysis of an experiment previously published (Mahon et al., 2013). Twenty-five University of Rochester undergraduate students (mean age = 20.1 years, SD = 1.2 years) participated in the study in exchange for payment. All participants had normal or corrected-to normal vision, were right-handed, and gave written informed consent in accordance with the University of Rochester Research Subjects Review Board.

2.2. Materials

Thirty-two grayscale photographs of tools and 32 animals were used; each item had two exemplars (for a total of 128 images). Scrambled versions of the stimuli were created to serve as a baseline condition; scrambled tools and animals were created by preserving (but randomly displacing) low-level visual information of each image. Stimulus presentation was controlled with 'A Simple Framework' (ASF; Schwarzbach, 2011) using the Psychophysics toolbox (Pelli, 1997) in MATLAB running on a MacPro. Within the bore of the magnet the images were back-projected onto a screen that was viewed with a mirror attached to the head coil.

2.3. Design and procedure

Participants passively viewed tool and animal stimuli in a miniblock design. Within each 16 s miniblock, 32 tools or 32 animals were presented for 500 ms each (ISI = 0 ms). Miniblocks with tool or animal stimuli were separated by 16 s of fixation. Each exemplar ($N=2$) was presented twice per run, and all images were repeated once per run as well, resulting in a total of 8 miniblocks of tools and animals; an additional 4 miniblocks of scrambled tools and animals were included in each run (order of miniblocks was random). All participants completed two runs of the category localizer experiment (213 volumes per run).

2.4. MR acquisition and analysis

Whole brain BOLD imaging was conducted on a 3 T Siemens MAGNETOM Trio scanner with a 32-channel head coil located at the Rochester Center for Brain Imaging. High-resolution structural T1 contrast images were acquired using a magnetization prepared rapid gradient echo (MP-RAGE) pulse sequence at the start of each session (TR = 2530, TE = 3.44 ms, flip angle = 7°, FOV = 256 mm, matrix = 256 × 256, 1 × 1 × 1 mm^3 sagittal left-to-right slices). An echo-planar imaging pulse sequence was used for T2* contrast (TR = 2000 ms, TE = 30 ms, flip angle = 90°, FOV = 256 × 256 mm^2, matrix = 64 × 64, 30 sagittal left-to-right slices, voxel size = 4 × 4 × 4 mm^3). The first two volumes of each run were discarded to allow for signal equilibration.

fMRI data were analyzed with the BrainVoyager software package (Version 2.0) and in-house scripts drawing on the BVQX toolbox written in MATLAB (wiki2.brainvoyager.com/BVQXtools). Preprocessing of the functional data included, in the following order, slice scan time correction (sinc interpolation), motion correction with respect to the first volume of the first functional run, and linear trend removal in the temporal domain (cutoff: 2 cycles within the run). Functional data were registered (after contrast inversion of the first volume) to high-resolution deskulled anatomy on a participant-by-participant basis in native space. For each participant, echo-planar and anatomical volumes were transformed into standardized space (Talairach & Tournoux, 1988). Functional data were smoothed at 6 mm FWHM (1.5 mm voxels), and interpolated to 3 × 3 × 3 mm^3 voxels.

2.5. Tool ROI definition

Tool-preferring voxels were identified in a whole brain analysis (random effects GLM; FDR corrected, $q < .05$) with the contrast of Tools > Animals (collapsing across the first and repeated presentations of stimuli within a run). Replicating previous studies (Chao et al., 1999; Chao & Martin, 2000; Mahon et al., 2007; Martin et al., 1996; Noppeney et al., 2006), viewing pictures of tools led to increased BOLD contrast in: the left posterior middle temporal gyrus, the left medial fusiform gyrus, and the left dorsal occipital cortex. The left ventral premotor cortex was localized by the contrast of Tools > Animals at a more lenient threshold of $p < .05$. The localization of the left parietal ROI was restricted to the first presentation of stimuli within a run to reduce the contribution of repetition suppression effects known to attenuate the BOLD signal in that region (Mahon et al., 2007; for review, see Grill-Spector, Henson, & Martin, 2006). Fig. 1 shows all of the voxels identified as exhibiting tool preferences in the whole brain analyses, and Table 1 lists coordinates and statistical values for the peak voxel from each ROI.

2.6. Functional connectivity analysis

The ROIs identified as exhibiting tool preferences were used as seeds and targets in a functional connectivity analysis. Specifically, the left medial fusiform gyrus, the left dorsal occipital cortex, the left ventral premotor cortex, and the left posterior middle temporal gyrus ROIs served as seeds, while the left parietal ROI served as the target ROI. All functional connectivity analyses were time course based, and used the time series from the entire run (2 runs per subject). While physiological recordings were not available for the current dataset (e.g., heart rate and breathing rate, see Gotts, et al., 2013; Gotts, et al., in press; Saad, et al., 2013), several sources of noise were regressed out of the time series data (after the preprocessing steps described above): (i) the change in head position across volumes, (ii) the global mean time course from the whole brain, and (iii) the time course from a ventricle. All functional connectivity analyses were then run over the

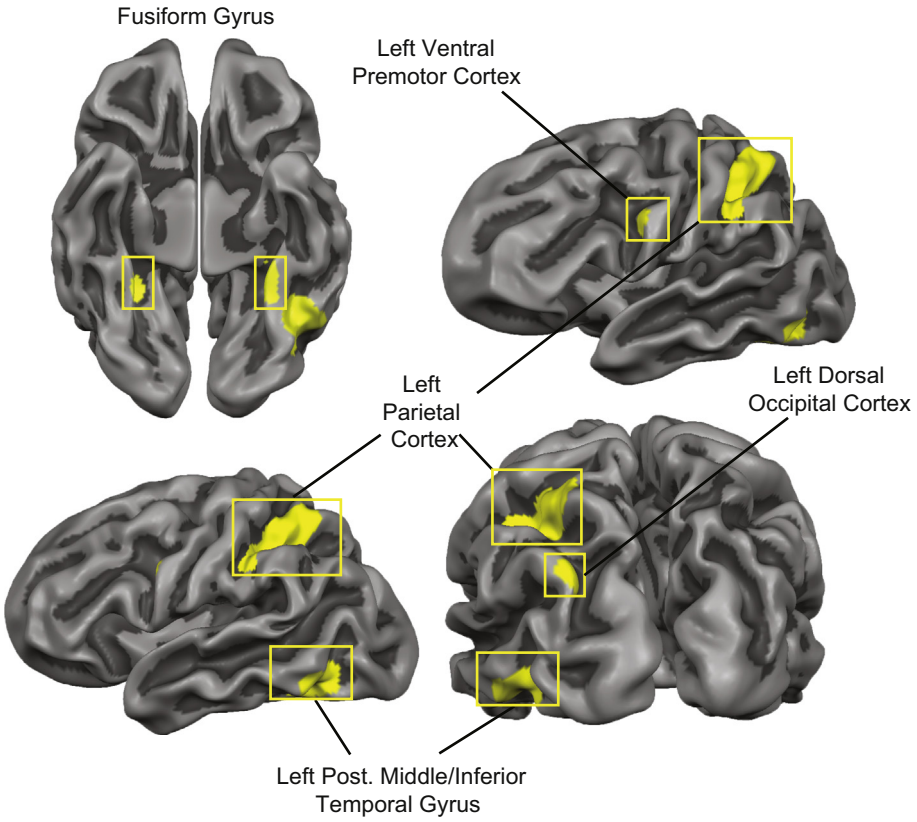

Fig. 1. Regions showing Tool Preferences in a whole-brain analysis (random effects). The regions identified included the left parietal lobule, the left dorsal occipital cortex, the left and right medial fusiform gyrus, the left posterior middle/inferior temporal gyrus, and the left ventral premotor cortex—all replicating previous findings (see text for discussion).

Table 1
Talairach coordinates for peak voxels from regions showing differential BOLD contrast for Tool stimuli.

Region	Peak voxel coordinates (*XYZ*)			Statistical value for peak voxel	Volume (mm^3)
Left parietal cortex	−43	−43	41	$t_{(24)}=6.14$, $p<.001$	6291
Left medial fusiform gyrus	−25	−44	−15	$t_{(24)}=6.64$, $p<.001$	1675
Left posterior middle temporal gyrus	−40	−62	−9	$t_{(24)}=6.40$, $p<.001$	3104
Left ventral premotor cortex	−49	−2	27	$t_{(24)}=2.47$, $p<.05$	184
Left dorsal occipital cortex	−31	−80	30	$t_{(24)}=4.28$, $p<.001$	389

residuals of that model. Whole-brain functional connectivity maps were restricted with a mask fit to the average deskulled Talairached anatomy.

The output from the whole brain functional connectivity analysis was a three-dimensional volume map, where each voxel contains a correlation value indexing the synchrony of the BOLD signal to the pre-determined seed region. One such volume map is generated for each run, for each subject, for each of the four seeds (i.e., $25\times2\times4=200$ whole brain connectivity maps). The two run-level volume maps for each seed by subject combination were then averaged. This allowed us to extract the voxel-wise correlation values from the left parietal cortex ROI ($n=233$ voxels), for each seed and for each subject. The resulting data were organized into four matrices (one for each seed), each matrix with 233 rows (corresponding to the voxels from parietal cortex) and 25 columns (corresponding to subjects). These matrices served as the inputs to the *k-means* clustering algorithm.

2.7. Connectivity-based k-means clustering analysis

A *k-means* clustering algorithm (using MATLAB) was used to cluster voxels from the parietal ROI on the basis of their similarity in functional connectivity to each of the four seeds across subjects, with each *k-means* solution constrained to 3 clusters (see above). Thus, four separate *k-means* solutions were generated (one for each seed); the output of each solution consisted of each voxel in parietal cortex being assigned to one of three clusters. The clustering solutions could then be visualized as maps, by assigning each cluster index a unique color. The first observation that emerged from the *k*-means clustering solutions was that there was a high degree of consistency in the spatial layout of the clusters. We color-coded the clusters in a way to highlight that similarity (see Supplemental Online Fig. 1). Specifically, there was always one cluster that was inferior and lateral to the other two, which we refer to as the Inferior Parietal ROI, and which we color-coded green. There was always another cluster superior and medial to the Inferior Parietal ROI, in the vicinity of anterior IPS, which we refer to as the Intraparietal Sulcus ROI, and which we color-coded red. Finally, the third cluster was, across the four seed-specific cluster maps, superior to the Inferior Parietal ROI and the Intraparietal Sulcus ROI; we refer to that cluster as the Superior Parietal ROI, and color-coded it blue (see Supplemental Fig. 1 for details).

Because we were interested in parcellating parietal cortex on the basis of its putative inputs from the ventral stream, the dorsal stream, and its output to motor cortex, and the status of the left posterior middle temporal gyrus as a ventral or dorsal stream region is somewhat equivocal (see above), we simplified the analysis in the following ways. First, in order to capture the consistency in the spatial layout of the clusters across the different *k-means* solutions for the different seeds, we took the intersection of the correspondingly color-coded clusters (see Fig. 2A). In the first level analysis we calculate this global intersection map using the left medial fusiform gyrus, left dorsal occipital cortex and left ventral premotor cortex as seeds—we can then use ROI-based functional connectivity to test for connectivity from the resulting parietal seeds to the left posterior middle temporal gyrus. To anticipate our finding, we observe that the left posterior middle temporal gyrus behaves, in terms of its functional connectivity to parietal cortex, very similarly as the left medial fusiform gyrus. Thus, and to substantiate this observation, in a second level analysis we determine the global level intersection map using as seeds, the left posterior middle temporal gyrus, the left ventral premotor cortex, and the left dorsal occipital cortex. This then allowed us to confirm, using ROI-based

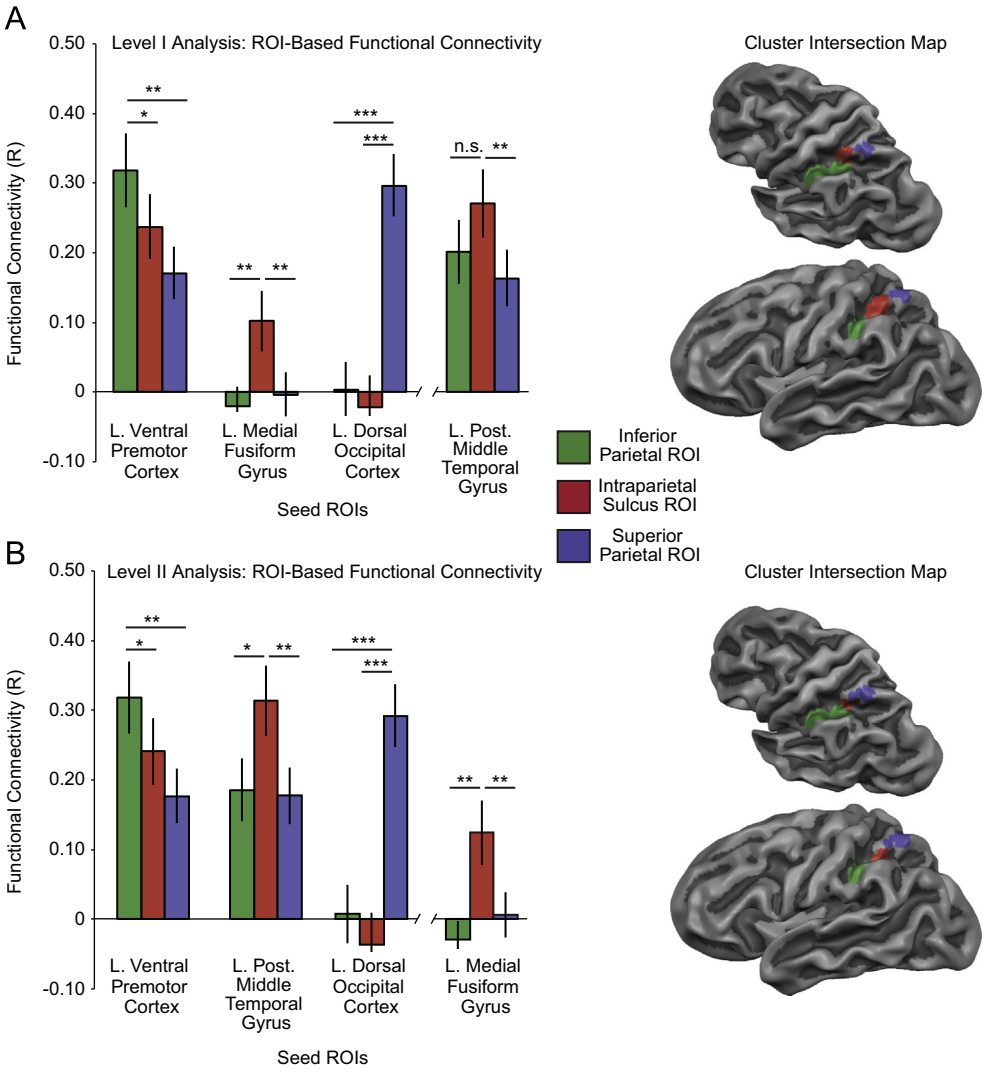

Fig. 2. *K-means* clustering solution: (A) the left medial fusiform gyrus was used as a seed from the ventral visual pathway. The cluster intersection map projected on the inflated surface of the left hemisphere is shown with the resulting clusters: Inferior Parietal ROI (green), the Intraparietal Sulcus ROI (red), and the Superior Parietal ROI (blue). The results of the ROI-based functional connectivity analysis indicate that the left Inferior Parietal ROI expressed privileged functional connectivity with ventral premotor cortex, the left Intraparietal Sulcus ROI expressed privileged functional connectivity with the left medial fusiform gyrus seed, and the left Superior Parietal ROI expressed privileged functional connectivity with left dorsal occipital cortex. (B) The left posterior middle temporal gyrus was used as a seed from the ventral visual pathway. The cluster intersection map is projected on the inflated surface of the left hemisphere. In the ROI-based functional connectivity analysis, the left Inferior Parietal ROI expressed privileged functional connectivity with the left ventral premotor cortex, the left Intraparietal Sulcus ROI expressed privileged functional connectivity with the left posterior middle temporal gyrus, and the left Superior Parietal ROI expressed privileged functional connectivity with the left dorsal occipital cortex. (*$p < .05$; **$p < .01$; ***$p < .001$). Error bars plot the standard error of the mean, across participants.

functional connectivity, that the left posterior middle gyrus' relation to parietal cortex is similar to that of the left medial fusiform gyrus.

3. Results

3.1. First level analysis: Using the left medial fusiform as the ventral stream seed

In the first analysis, we took the intersection of the *k-means* solutions that were generated when using the left ventral premotor cortex, the left dorsal occipital cortex, and the left medial fusiform gyrus as seed regions (see Fig. 2A for an intersection map). We then recomputed functional connectivity between each of the three parietal clusters and the original seed ROIs—this allowed us to determine the functional connectivity preferences of each of the parietal clusters that were generated by the *k-means* algorithm. In other words, the *k-means* clustering solution tells us that the connectivity profiles of the resulting parietal clusters are dissociable, but does not tell us which parietal ROI exhibits privileged connectivity to which seed. This is because we used *k-means* clustering with 3 clusters, and *k-means* maximizes the distance between clusters, and minimizes the distance within clusters (cf., Mirkin, 2005). Thus, the ROI-based functional connectivity analysis is not a substantively different analysis from the *k-means* clustering solution itself—it merely provides a basis with which to interpret the clusters that were generated. The results of the ROI-based functional connectivity analyses, shown in the bar plot of Fig. 2A, indicated a triple order interaction between the factors Seed Region and Parietal Cluster ($F(4.16, 99.85) = 21.05$, $p < .001$).

- The Inferior Parietal ROI (colored green in Fig. 2A; Talairach coordinates: −43, −43, 33) expressed stronger functional connectivity with the left ventral premotor cortex than did the Intraparietal Sulcus ROI (red cluster; $t(24) = 2.26$, $p < .05$) or the Superior Parietal ROI (blue cluster; $t(24) = 3.05$, $p < .01$; see Fig. 2A).

Table 2
Talairach coordinates for the left parietal clusters identified with *k-means* analyses over functional connectivity data. Talairach coordinates correspond to center of mass.

Region	Center of mass coordinates (*XYZ*)			Volume (mm^3)
Level I analysis				
Inferior parietal ROI	−43	−43	33	1647
Intraparietal sulcus ROI	−32	−48	42	567
Superior parietal ROI	−34	−58	50	594
Level II analysis				
Inferior parietal ROI	−44	−43	34	1674
Intraparietal sulcus ROI	−31	−49	40	297
Superior parietal ROI	−34	−58	47	675

- The Intraparietal Sulcus ROI (colored red in Fig. 2A, Talairach coordinates: −32, −48, 42) expressed stronger functional connectivity with the left medial fusiform gyrus than did the Inferior Parietal ROI ($t(24)=2.90$, $p<.01$) or the Superior Parietal ROI ($t(24)=3.41$, $p<.01$; see Fig. 2A).
- The Superior Parietal ROI (colored blue in Fig. 2A, Talairach coordinates: −34, −58, 50) expressed stronger functional connectivity with left dorsal occipital cortex than did either the Inferior Parietal ROI ($t(24)=6.12$, $p<.001$) or the Intraparietal Sulcus ROI ($t(24)=8.09$, $p<.001$; see Fig. 2A; see Table 2 for parietal cluster details).

As can be seen (right most panel in bar plot of Fig. 2A), when we computed ROI-based functional connectivity between the left posterior middle temporal gyrus and the three parietal clusters, the pattern was most similar to that obtained for the left medial fusiform gyrus. In other words, even though the left posterior middle temporal gyrus was not used (at all) in the *k-means based* definition of the parietal clusters, the connectivity profile of those clusters indicates that the left posterior middle temporal gyrus has a relationship to those parietal regions that is most similar to that of the left medial fusiform gyrus. To further substantiate this observation, we repeated the entire analysis, this time using the left posterior middle temporal gyrus explicitly as a seed, while not using the left medial fusiform gyrus as a seed, in the *k-means* definition of the parietal clusters.

3.2. Second level analysis: Using the left posterior middle temporal gyrus as a ventral stream seed

We repeated the entire *k-means* clustering analysis, using as seeds the left posterior middle temporal gyrus as the surrogate seed for inputs to parietal cortex from the ventral stream, as well as the left dorsal occipital cortex and left ventral premotor ROIs. The first observation is that the organization of the resulting parietal clusters that emerged from the global intersection across the *k-means* solutions from the three seeds is almost exactly the same as what was observed in the first level analysis above. The results of the ROI-based functional connectivity analysis are plotted in Fig. 2B. As expected, again, a triple-order dissociation in functional connectivity was present among the three clusters within left parietal cortex and the three seed regions ($F(4.26, 102.14)=21.52$, $p<.001$). The patterns of ROI-based functional connectivity were remarkably similar to the first level analysis—in other words, the left posterior middle temporal gyrus and the left medial fusiform gyrus behaved similarly in terms of the their connectivity to parietal cortex. Specifically:

- The Inferior Parietal ROI (colored green, Talairach coordinates: −44, −43, 33) expressed stronger functional connectivity with the left ventral premotor cortex than the Intraparietal Sulcus ROI ($t(24)=2.22$, $p<.05$) or the Superior Parietal ROI ($t(24)=2.99$, $p<.01$).
- The Intraparietal Sulcus ROI (colored red; Talairach coordinates: −31, −49, 40) expressed stronger functional connectivity with the left posterior middle temporal gyrus than did the Inferior Parietal ROI ($t(24)=3.43$, $p<.01$) or the Superior Parietal ROI ($t(24)=3.64$, $p<.01$).
- Finally, the Superior Parietal ROI (colored blue, Talairach coordinates: −34, −58, 50) expressed stronger functional connectivity with the left dorsal occipital cortex than did the Inferior Parietal ROI ($t(24)=6.02$, $p<.001$) or the Intraparietal Sulcus ROI ($t(24)=7.79$, $p<.001$).

As for the first level analysis, we also computed ROI-based functional connectivity between the three parietal clusters and the left medial fusiform gyrus (which was not used in the definition of the parietal clusters). Substantiating the pattern observed above, the left medial fusiform gyrus and the left posterior middle gyrus exhibited highly similar patterns of functional connectivity to the three parietal regions (see Fig. 2B and Table 2 for parietal cluster details).

3.3. Analysis of possible differences in BOLD amplitudes across parietal clusters

The functional connectivity patterns we observed cannot be explained by biases introduced by ROI selection because the core phenomenon is a triple-order dissociation in functional connectivity over the same dataset—hence entirely orthogonal to (any) contrast used to define the regions. Nevertheless, we sought to test whether the same or a similar interaction would be present across the clusters when looking at differential BOLD contrast elicited by viewing tool stimuli compared to animal stimuli (see Table 3). In order to avoid possible problems of comparing BOLD signal across different regions, which may have different hemodynamic response functions (HRF), we used a deconvolution analysis (i.e., finite impulse response) that makes no assumptions about the shape of the HRF. A deconvolution analysis is thus not susceptible to differences in timing and fit of a modeled HRF to the experimental predictors in different regions (because no HRF is modeled).

We extracted beta values from the parietal clusters for the eight volumes following each miniblock onset (i.e., 16 s), and entered them into a repeated-measures ANOVA with the factors Cluster (Inferior Parietal/Intraparietal Sulcus/Superior Parietal), Category (tool/animal), and Volume (TRs 1–8). Two separate ANOVAs were run, corresponding to whether the left medial fusiform gyrus or the left posterior middle temporal gyrus was used as the surrogate ventral stream seed to define parietal clusters (i.e., corresponding to Levels I and II analyses above). When parietal clusters were defined using the left medial fusiform gyrus as the ventral stream seed, there were significant main effects of Volume ($F(1.95, 46.88)=6.86$, $p<.01$) and Condition ($F(1, 24)=8.28$, $p<.001$). However, and importantly, there was no significant interaction between Cluster

Table 3
BOLD amplitude for parietal clusters derived with *k-means*.

Defining seed	Mean BOLD amplitude	SEM (across subjects)
Level I analysis		
Inferior parietal ROI	.17	.06
Intraparietal sulcus ROI	.38	.11
Superior parietal ROI	.30	.09
Level II analysis		
Inferior parietal ROI	.16	.06
Intraparietal sulcus ROI	.42	.12
Superior parietal ROI	.31	.09

and Condition ($F<1$), indicating that the three parietal clusters all showed uniformly strong responses to tool stimuli compared to animal stimuli. The same pattern emerged when the parietal clusters were defined using the left posterior middle temporal gyrus as the surrogate ventral stream seed (main effect of Volume $F(1.96, 47.05)=6.59$, $p<.01$, main effect of Condition $F(1, 24)=24.40$, $p<.001$; no interaction between Condition and Cluster ($F<1$), indicating once again that the three parietal clusters showed uniformly robust activation for tool stimuli).

3.4. Control analyses

One concern that may arise with the analysis approach that we have taken is that the 'baseline' is unknown for the likelihood that clusters of the size we have reported could be observed by chance. In other words, given random data, what is the likelihood of observing clusters—i.e., sets of contiguous voxels? We believe that an explanation that assumed the parietal clusters arose from chance 'lumpiness' in the data is extremely unlikely, precisely because of the tight alignment between the anatomical location of our clusters and previous parcellation schemes of left parietal cortex (see Section 4 below). Nevertheless, we sought to estimate what the 'baseline level of lumpiness' would be in random data. In other words, setting aside the likelihood of observing anatomical alignment of our clustering solution with the known functional anatomy of parietal cortex, we sought to reject the more modest objection that clusters of the size we have reported could arise due to chance. A fortiori, rejecting an explanation of the *size* of the clusters as arising from chance implies rejection of the claim that the anatomical distribution of clusters of that size *and* in that particular arrangement could arise by chance. To that end, we carried out a Monte Carlo style permutation test, the goal of which was to show that the clusters displayed in Fig. 2 would be outside of the range of likely outcomes if the same analysis approach were applied to randomly shuffled data.

Permutation tests were run for each seed region's functional connectivity values in left parietal cortex. Thus, each of the original four matrices of voxel rows by subject columns served as the inputs to the simulation of chance. For each matrix, the rows were randomly shuffled for each individual column, and then the new (shuffled) matrix was entered into a *k-means* clustering analysis, using the same parameters as the analysis of the 'real' data. These "chance simulations" were carried out 10,000 times for each seed matrix. In order to obtain a global measure of lumpiness, we calculated the Euclidean distances among (i) all within-cluster voxels, and (ii) all between-cluster voxels. The logic here is that for 'real' clusters (i.e., those shown in Fig. 2A and B), the average within-cluster Euclidian distance (among voxels) will be lower than the average between-cluster Euclidian distance (among voxels). This is because the clusters present in the 'real' data picked out sets of contiguous voxels. In contrast, the clusters that are outputted from random data would not have a bias to be composed of contiguous voxels, except for what would arise due to 'chance.' In this way the measure of Euclidian distance provides an estimate of the 'lumpiness' that would be expected from randomly shuffled 'real' data. This calculation of Euclidian distance was performed for each solution generated by the permutation test.

For each seed region there were 10,000 values for the mean within-cluster distance (distance among all pairs of voxels, for those pairs where the two voxels were in the same cluster), and 10,000 values for the mean between-cluster distance (distance among all pairs of voxels for those pairs where the two voxels were in different clusters; see Supplemental Fig. 2 for the Euclidean distance distributions). In Fig. 3 there are four columns with distributions corresponding to the four seed regions. In panel A, the distributions of within-cluster Euclidean distances and between-cluster Euclidean distances for the simulated data are plotted as histograms, and are overlaid on top of each other. The within-cluster and between-cluster Euclidian distance distributions associated with the 'real' data are plotted as histograms in panel B. It is important to note that the within-cluster distributions for the 'real' data minimally overlapped with the between-cluster distributions, which is represented by plotting the mean magnitude of the Euclidean distance differences in Fig. 3C.

Also noteworthy, the permutation test had the power to identify subtle "lumpiness" within the data, as the means for the difference distributions over the randomly shuffled data are all shifted slightly but significantly rightward (one-sample *t*-test, all p's $<.001$; see Supplemental Fig. 2). These analyses therefore indicate that while there is a minimal amount of 'lumpiness' present in random data, the voxel contiguity that is present in the clusters generated over the 'real' data is far outside what could be attributed to chance.

4. General discussion

The goal of this study was to provide a new empirical basis for bringing into alignment existing anatomically-based parcellation schemes of the inferior parietal lobule with the patterns of functional activation associated with viewing tools. As noted in Section 1, when participants view images of tools, compared to comparable baseline categories (e.g., animals, vehicles), a large swath of left parietal cortex is activated, that extends from the supramarginal gyrus dorsally to the anterior IPS, and posteriorally to posterior parietal cortex (Lewis, 2006). We replicated this observation within the context of our study, and then sought to parcellate left parietal tool preferring voxels on the basis of their functional connectivity to extra-parietal brain regions that also express differential BOLD contrast for tool stimuli. *k-Means* clustering was used to organize voxels in left parietal cortex on the basis of their similarity in functional connectivity to the ventral stream (left medial fusiform gyrus/left posterior middle temporal gyrus), the dorsal stream (left dorsal occipital cortex), and the motor system (left ventral premotor cortex). This approach, in conjunction with an ROI-based functional connectivity analysis, revealed a triple-order dissociation in functional connectivity among three subregions within left parietal tool preferring regions. We further found that the left posterior middle temporal gyrus behaves, in terms of its connectivity to left parietal cortex, more like a ventral stream region than like a dorsal stream region. Finally, control analyses demonstrated that the obtained pattern of functional connectivity-based clustering of parietal tool representations was far outside the range of what would be expected by chance. In the next section we formally compare our parcellation scheme of left parietal cortex to two parcellation schemes that have subdivided the inferior parietal cortex on anatomical grounds.

4.1. Alignment of different approaches for parcellating parietal cortex

There is a long history of fine-grained anatomical parcellations of parietal cortex in human and non-human primates. Brodmann (1909) classically divided the inferior parietal lobule into the supramarginal (BA 40) and angular gyrus (BA 39), and the superior parietal lobule into BA 5 and BA 7. Subsequent investigations further parcellated the inferior parietal lobule into distinct subregions (e.g., see Matelli, Luppino, & Rizzolatti, 1985; Matelli, Luppino, & Rizzolatti, 1991; Pandya & Kuypers, 1969; Vogt & Vogt, 1919; von Economo, 1929). For instance, von Economo (1929) showed that the inferior parietal lobule could be subdivided into areas PFop, PFt, PFcm, PF, PFm, and PG; those regions were approximately organized along a rostral-to-caudal axis within the supramarginal and angular gyri (see

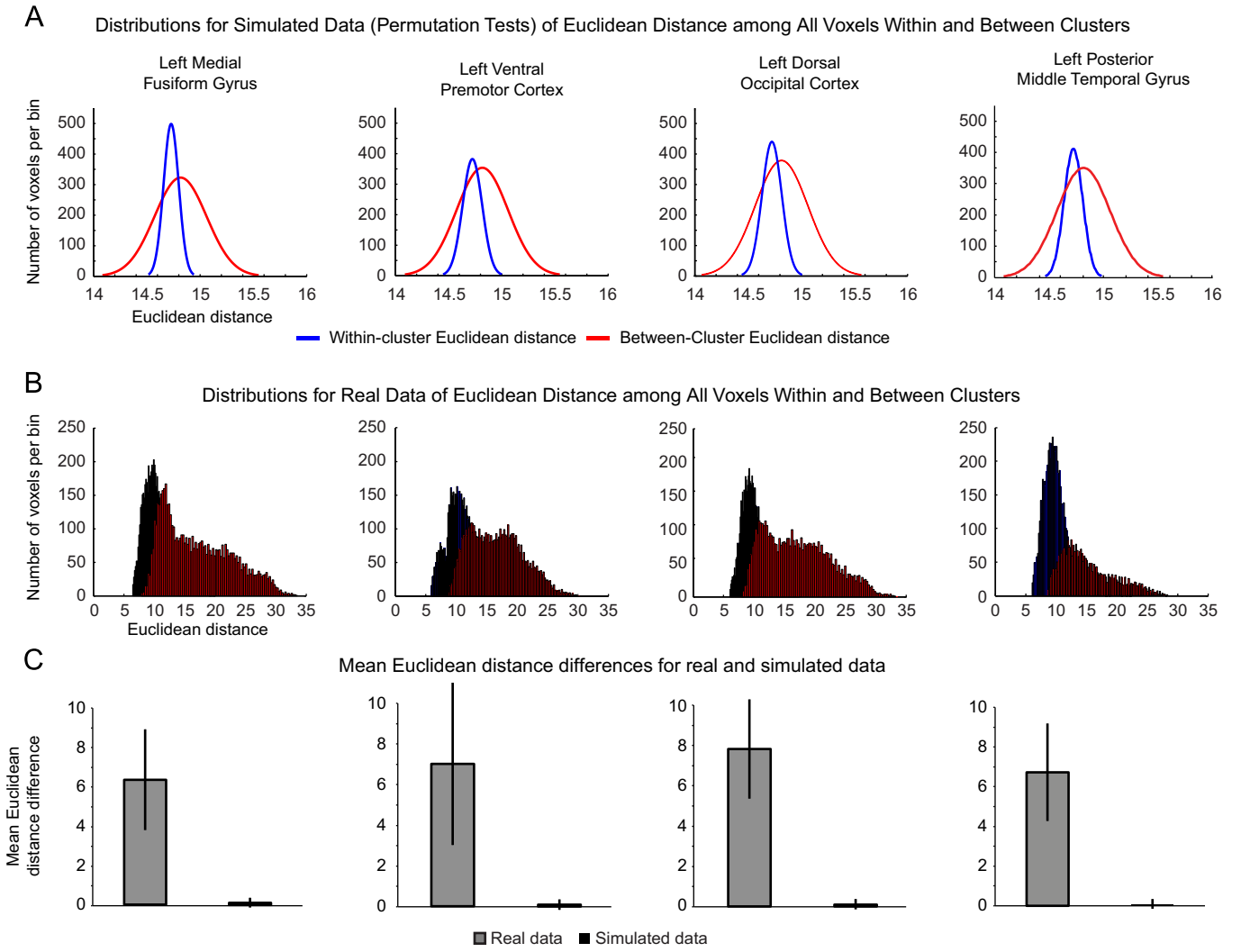

Fig. 3. Permutation tests for the likelihood of observing clusters. (A) The histograms plot the distribution of between-cluster and within-cluster Euclidean distances for analyses over randomly shuffled data (see also Supplemental Fig. 2 for further analyses involving the simulated data). (B) In order to have a principled way of comparing the Euclidean distance difference between the within- and between-cluster voxel pairings for the 'real' data, we pooled all within-cluster Euclidean distances (collapsing across clusters) into one distribution (blue), and we pooled all between-cluster Euclidean distances (collapsing across clusters) into a second distribution (red). (C) The mean magnitude difference among all within- and between-cluster voxel pairs are plotted for 'real' and simulated data. Because 'real' clusters were of different sizes, we took the average within-cluster distance, and subtracted that value from two separate between-cluster values in order to obtain a mean Euclidean distance difference (i.e., to calculate the mean Euclidean distance, we computed all pairwise Euclidean distances among voxels in the three parietal clusters, then subtracted the mean distance among all voxels in different clusters from the mean distance among all voxels in the same cluster). The same approach was taken for the simulated data. Error bars represent standard deviation over the three mean Euclidean distance difference scores.

also von Economo & Koskinas, 1925). Pandya and Seltzer (1982) provided one of the first detailed analyses of the dense interconnections among areas within the macaque inferior parietal lobule. In their parcellation, they argued that the macaque inferior parietal lobule contained four subregions, areas PF, PFG, PG, and Opt, which are located, respectively, along a rostral-to-caudal axis in the inferior parietal lobule.

Recently, Caspers et al. (2013) have provided a new parcellation scheme for the inferior parietal lobule that includes and extends, and thus arguably supersedes, previous parcellation schemes. Caspers and colleagues used autoradiographic labeling of receptors in post-mortem brains to parcellate the inferior parietal lobule into three distinct clusters: The first, rostral-most cluster, is in the vicinity of PFop, PFcm, and PFt, in the supramarginal gyrus; the second cluster lies in an intermediate zone, and overlaps with PF and PFm, and lies along the lateral bank of the IPS; the third, caudal-most cluster, is in the vicinity of posterior PG (PGa and PGp), near the angular gyrus (see Caspers et al., 2013, Fig. 8D therein). This partition of the inferior parietal lobule aligned well with previous work from the same group using laminar distribution analyses (Caspers et al., 2006), and probabilistic tractography (Caspers et al., 2011; see also Mars et al., 2011). Ruschel et al. (in press) also reported a similar rostral-to-caudal arrangement of three clusters within the human inferior parietal lobule after parcellating the region using probabilistic tractography; their clusters included inferior parietal cortex anterior (IPCa) in the supramarginal gyrus, IPCp (posterior) in the angular gyrus, and IPCm (middle) in an intermediate area that overlaps with the rostral portion of the angular gyrus and caudal portion of the supramarginal gyrus.

While the studies just discussed (Caspers et al., 2013, 2006, 2011; Ruschel et al., in press) parcellated parietal cortex using anatomical analyses, Konen and Kastner (2008) used a delayed saccade task to localize four topographically organized areas of the IPS: two areas were located in the posterior portion of the IPS (IPS1, IPS2) and two areas were located in the anterior portion of the IPS (IPS3, IPS4). The authors then carried out a series of fMRI-adaptation (fMR-a) experiments to show that neural responses within areas IPS1 and IPS2 showed adaptation to (i) repeated presentations of images and (ii)

Table 4
Abbreviations of functionally- and anatomically-defined parietal subregions.

Brodmann areas	Superior parietal lobule		Inferior parietal lobule				
	BA 5	BA 7	BA 39		BA 40		
von Economo (1929)	Inferior parietal lobule						
	PFop	PFt	PFcm		PFm	PG	
Caspers et al. (2013)	Inferior parietal lobule						
	PFop	PFt	PFcm	PF	PFm	PGa	PGp
Ruschel et al. (in press)	Inferior parietal lobule						
	IPCa	IPCm	IPCp				
Konen and Kastner (2008)	Posterior IPS		Anterior IPS				
	IPS1	IPS2	IPS3	IPS4			

transformations in size, form (e.g., 2D or 3D), and viewpoint. Interestingly, Konen and Kastner did not find similar patterns of neural activity in IPS3 and IPS4. It is important to note that Konen and Kastner's parcellation of parietal cortex does not conflict with that of Caspers and colleagues and Ruschel and colleagues, because Konen and Kastner's study is largely concerned with superior and posterior parietal regions (IPS1–4), while Caspers and colleagues and Ruschel and colleagues focused on the inferior parietal lobule (see Table 4 for a complete list of abbreviations).

4.2. Direct comparison of functional connectivity based parietal clusters with anatomical parcellation schemes

We then sought to provide a more formal and direct comparison between the parietal clusters identified on the basis of functional connectivity of parietal cortex with the anatomically-based parcellation scheme proposed by Caspers et al. (2013) and Ruschel et al. (in press). For simplicity, we restrict the analyses to the parietal clusters obtained when using the left medial fusiform gyrus as the ventral stream seed (and because the results are qualitatively identical swapping the left posterior middle temporal gyrus for the left medial fusiform gyrus). We computed ROI-based functional connectivity among the parietal clusters we reported above (Inferior Parietal ROI, Intraparietal Sulcus ROI, and Superior Parietal ROI) and the parietal clusters from Caspers et al. (2013) and Ruschel et al. (in press). The results are shown in Fig. 4. Panel A of Fig. 4 is a projection of the left parietal tool clusters we have reported with the parietal clusters from Caspers et al. (2013). As can be seen, there is partial overlap between the left parietal parcellation scheme we have reported, and the anatomical layout of the clusters from Caspers and colleagues' parcellation scheme.

In order to ensure that our projection of Caspers et al. (2013) parietal regions was correct, and to compare our connectivity-based parietal parcellation scheme with the anatomical parcellation scheme of Caspers and colleagues, we used hierarchical clustering to determine the relative similarity in functional connectivity among all parietal clusters in Fig. 4A (see Caspers et al., 2013, Fig. 8A therein). Fig. 4B shows the results of these hierarchical clustering analyses in the form of dendrograms. Critically, we replicate the main patterns of the inferior parietal parcellation scheme from Caspers et al. (2013) using functional connectivity over the present dataset (see Supplemental Fig. 3). The inferior parietal clusters first divide into two groups: areas PFop, PFt, PFcm and PF clustered together, while PFm, PGa and PGp clustered together. This overall pattern is similar to Caspers and colleagues partition scheme, where areas PFcm, PFop, and PFt comprised one cluster, areas PGa and PGa comprised a second cluster, and areas PF and PFm comprised a third cluster (see Caspers et al., 2013, Fig. 8A). We then repeated the analysis (Fig. 4B, left panel), including the left parietal tool clusters that we have identified. Area PF was grouped with the clusters in anterior and lateral portions of the inferior parietal lobule (Inferior Parietal ROI; Intraparietal Sulcus ROI), while the Superior Parietal ROI was most similar to regions within caudal IPL and the angular gyrus (PGa, PGp, PFm).

The clustering of the Inferior Parietal ROI with PF is consistent with human and non-human anatomical studies that have mapped the dense reciprocal connections between anterior intraparietal regions and premotor cortex (Borra et al., 2008; Caspers et al., 2011; Mars et al., 2011; Rizzolatti & Matelli, 2003; Rozzi et al., 2006; Rushworth et al., 2006). The Inferior Parietal ROI likely overlaps Caspers and colleagues' PF and PFt and Ruschel and colleagues' IPCa.

The Intraparietal Sulcus ROI cluster is in the vicinity of Caspers and colleagues' PF and PFm; it is superior and medial to the Inferior Parietal cluster and anterior and inferior to the Superior Parietal cluster. The anatomical location of the Intraparietal Sulcus cluster and its functional connectivity with the ventral stream is consistent with human and non-human primate anatomical experiments which have mapped anatomical projections between AIP of the inferior parietal lobule and ventral temporal cortex (e.g., see Borra et al., 2008, 2010; Caspers et al., 2011; Rozzi et al., 2006; Ruschel et al., in press; Zhong & Rockland, 2003). In this context it is important to note that a number of tracing studies in macaques have shown that AIP and F5 (i.e., ventral premotor) have strong reciprocal connections; our findings are not necessarily in conflict with that observation because here we are highlighting how the parietal clusters differ in their connectivity to the ventral stream.

The Superior Parietal cluster was most similar to caudal IPL regions PGa, PGp, and PFm. While the superior parietal lobule was not included in Caspers et al.'s (2013) parcellation scheme, it should be noted that the Superior Parietal cluster likely overlaps with IPS 3 and 4 (Konen & Kastner, 2008), two regions that are important for visually guided reaching and grasping (Cavina-Pratesi et al., 2007; Culham et al., 2003; Konen et al., 2013), and which are typically damaged in optic ataxic patients with reaching impairments. In this context, it is significant that we observed the Superior Parietal cluster to exhibit privileged functional connectivity to the left dorsal occipital cortex seed (see also Culham et al., 2003 for relevant data and discussion).

In a second analysis, we used hierarchical clustering to directly compare the parcellation scheme of Ruschel and colleagues with the left parietal tool clusters we have reported. We find that their area IPCa is grouped with the Inferior Parietal cluster; additionally, Ruschel and colleagues' areas IPCm and IPCp were found to group together in a separate cluster (Fig. 4B, right panel). The clustering of IPCa with the Inferior Parietal cluster is consistent with the tractography findings of Ruschel and colleagues, as IPCa was found to express strong structural connectivity with the motor system (see also Mars et al., 2011; Rushworth et al., 2006). Perhaps surprisingly, our Superior Parietal cluster, which showed the strongest functional connectivity to the left dorsal occipital cortex, did not cluster with Ruschel and colleagues' region (IPCp) that

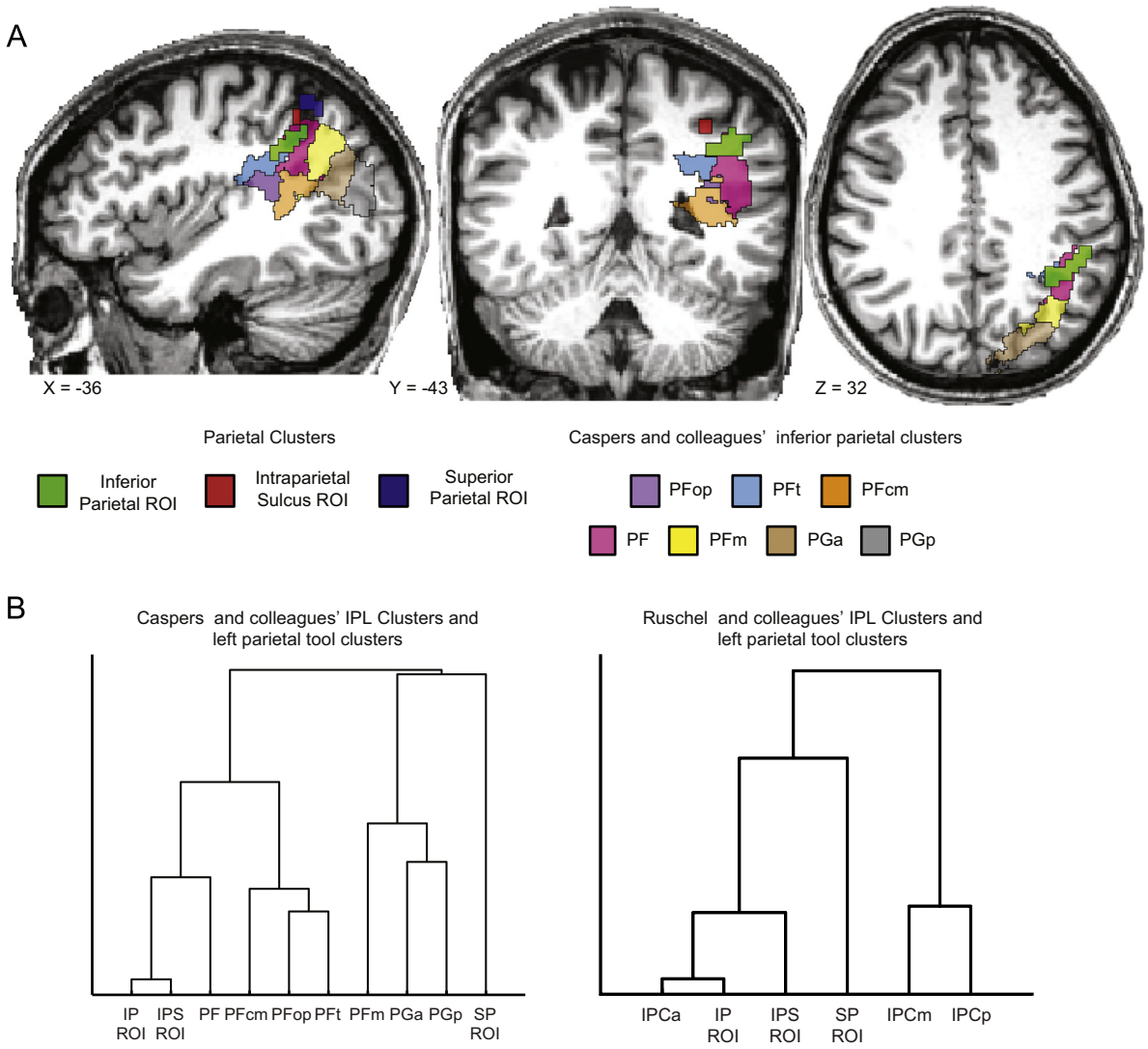

Fig. 4. Comparison of Caspers and colleagues' anatomical parcellation scheme, Ruschel and colleagues' anatomical parcellation scheme, and the parietal clusters we have reported: (A) overlap between our parietal clusters and the clusters reported by Caspers et al. (2013). The Inferior Parietal ROI partially overlaps with areas PFt and PF; the Intraparietal Sulcus ROI minimally overlaps with area PF; the Superior Parietal ROI does not overlap with any of the anatomically-based inferior parietal clusters, but likely overlaps with regions IPS3 and/or IPS4 from Konen and Kastner (2008). (B) Dendrograms representing the similarity in functional connectivity among the anatomically-derived clusters of Caspers and colleagues and the left parietal clusters we reported (left panel), and among the DTI-based clusters of Ruschel and colleagues and the left parietal clusters we reported (right panel).

showed the strongest structural connectivity with the superior parietal lobule. This points to the need for direct and within-subject analyses that use both DTI and functional connectivity.

4.3. The contribution of Euclidian distance to inter-cluster connectivity

A final issue that needs to be addressed concerns the anatomical distance among clusters and how that may affect their functional connectivity. It is important to emphasize that, if there is a relationship between anatomical distance and functional connectivity, this does not necessarily mean that the functional connectivity effects are 'mere artifacts' of anatomical distance. It would remain an empirical question as to whether, for this set of brain regions, there is greater inter-region connectivity for regions that are closer together. Nevertheless, to address this issue empirically within our own data, we computed the anatomical Euclidian distance among the centers of mass of all ROIs (seeds and parietal clusters). We found that anatomical distance was negatively correlated with functional connectivity: as the Euclidean distance between two ROIs decreased, functional connectivity increased (see Supplemental Fig. 4, left panel). We thus regressed anatomical distance from functional connectivity values, and used hierarchical clustering to again group the regions, this time using the residuals from the regression model. Importantly, the patterns in Fig. 4B were largely preserved after having regressed out anatomical distance (see the right panel of Supplemental Fig. 4). This finding is important as it indicates that, over and above effects of anatomical distance, there is consistency in the hierarchical clustering organization of the parietal clusters we have reported and previous anatomically defined parcellation schemes (e.g., Caspers et al., 2013; Ruschel et al., in press).

5. A novel framework for understanding the causes of upper limb apraxia

Our results, together with the neuropsychological data reviewed in Section 1, indicate substantial heterogeneity in the left parietal areas that show uniformly high BOLD responses when

viewing manipulable objects. Patient evidence has shown that damage to left lateral and inferior parietal cortex is associated with upper limb apraxia, while damage to superior and posterior parietal cortex is associated with optic ataxia. Our functional connectivity analyses dovetail with the patient evidence by showing that tool-preferring regions of parietal cortex can be parcellated according to connectivity with the ventral stream, dorsal stream, and motor system. In the context of the current investigation, it is important to note that participants were not asked to overtly use tools while in the scanner, and it remains an exciting, and important open issue, as to how connectivity within the Tool Processing Network might change dynamically as a function of task: for instance, asking participants to free-view manipulable objects, versus pantomime object use, versus manipulate actual objects during scanning. Because the participants in our study were passively viewing the stimuli, our design allows us to develop hypotheses about the broader set of regions that are involved in tool processing, and how lesions to subregions (i.e., clusters) within parietal clusters may explain different patterns observed in upper limb apraxia.

The three clusters that we have identified in tool-responsive left parietal cortex are similar to regions identified on the basis of anatomical parcellation schemes of the parietal lobe. Using a hierarchical clustering analysis we found that the functional connectivity profile for the Inferior Parietal ROI and the Intraparietal Sulcus ROI was most similar to Caspers and colleagues' area PF and Ruschel and colleagues' area IPCa, and the Superior Parietal ROI was most similar to Caspers and colleagues' caudal IPL regions, in the vicinity of the angular gyrus. It is also important to note that the Superior Parietal ROI lies in close proximity to Konen and Kastner's IPS 3 and 4, two regions that are relevant for visually guided reaching and grasping.

An interesting avenue for future work will be to adopt a combination of functional and structural connectivity analyses to measure the degree to which the patterns of functional connectivity among brain regions depend on direct white matter pathways. Where there is anatomical connectivity there is functional connectivity, but the reverse is not true—there can be functional connectivity between regions that do not have a direct white matter projection. Thus, the interesting issue that arises concerns regions that exhibit functional but not anatomical connectivity. In that case, the question arises as to what are the 'third party' regions that mediate functional connectivity between those regions? Such an approach would be relevant for testing whether the types of neurological impairments that have classically been associated with parietal damage, are in fact due to the parietal lesions, or instead to the fact that connectivity between parietal and extra-parietal regions, or even connectivity among extra-parietal regions has been disrupted. Important precedent on this type of phenomenon is provided by hemispatial neglect. Hemispatial neglect was long associated with right inferior parietal lesions, but subsequently shown to critically depend on disconnection of parietal and frontal regions (e.g., He et al., 2007; Thiebaut de Schotten et al., 2005).

In the context of tool representations in the left parietal cortex, our findings frame the possibility that some aspects of limb apraxia may derive not only from the parietal insult itself. Rather, some types of impairment observed in limb apraxia may be due to disconnection of parietal regions from regions of the temporal lobe that represent object concepts, or from the disconnection of parietal regions from regions of the fronto-motor system. More specifically, this framework predicts that disconnection between parietal and temporal cortices, without frank damage to parietal action representations, could give rise to errors of content in object use (using a toothbrush like a butter knife with a well formed and spatiotemporally coherent action). In contrast, disconnection of parietal action representations from frontal motor structures could give rise to spatiotemporal errors—errors of object use that are correct in terms of their content, but disorganized and kinematically disfluent. A similar theoretical approach was suggested by Geschwind (1965), whereby differential disconnections among the visual system, the motor system, and left hemisphere language areas would give rise to the different errors that apraxic patients commit when asked to imitate and pantomime meaningful action. Future work combining voxel-based lesion symptom mapping, probabilistic DTI, detailed cognitive evaluations, and fMRI-based connectivity in large cohorts of left brain damaged patients would permit direct evaluation of these new hypotheses.

Acknowledgments

We would like to thank Elon Gaffin-Cahn and David Paul for technical assistance, Svenja Caspers for sharing the NIFTI files of her group's parietal clusters, and Michael Ruschel for making his group's parietal clusters available. Preparation of this manuscript was supported in part by NINDS grant NS076176 to B.Z.M., and by the University of Rochester Center for Visual Science pre-doctoral training fellowship (NIH training Grant 5T32EY007125-24) to F.E. G. This research was also supported in part by Norman and Arlene Leenhouts.

Appendix A. Supporting information

Supplementary data associated with this article can be found in the online version at: http://dx.doi.org/10.1016/j.neuropsychologia.2014.05.018.

References

Almeida, J., Mahon, B. Z., Nakayama, K., & Caramazza, A. (2008). Unconscious processing dissociates along categorical lines. *Proceedings of the National Academy of the Sciences of the United States of America*, *105*, 15214–15218.

Almeida, J., Mahon, B. Z., & Caramazza, A. (2010). The role of the dorsal visual processing stream in tool identification. *Psychological Science*, *21*, 772–778.

Almeida, J., Fintzi, A. R., & Mahon, B. Z. (2013). Tool manipulation knowledge is retrieved by way of the ventral visual object processing pathway. *Cortex*, *49*, 2334–2344.

Beauchamp, M. S., Lee, K. E., Haxby, J. V., & Martin, A. (2002). Parallel visual motion processing streams for manipulable objects and human movements. *Neuron*, *34*, 149–159.

Beauchamp, M. S., Lee, K. E., Haxby, J. V., & Martin, A. (2003). fMRI responses to video and point-light displays of moving humans and manipulable objects. *Journal of Cognitive Neuroscience*, *15*, 991–1001.

Bedny, M., Caramazza, A., Pascual-Leone, A., & Saxe, R. (2012). Typical neural representations of action verbs develops without vision. *Cerebral Cortex*, *22*, 286–293.

Binder, J. R., Desai, R. H., Graves, W. W., & Conant, L. L. (2009). Where is the semantic system? A critical review and meta-analysis of 120 functional neuroimaging studies. *Cerebral Cortex*, *19*, 2767–2796.

Binkofski, F., Buccino, G., Posse, S., Seitz, R. J., Rizzolatti, G., & Freund, H.-J. (1999a). A fronto-parietal circuit for object manipulation in man: Evidence from an fMRI-study. *European Journal of Neuroscience*, *11*, 3276–3286.

Binkofski, F., Buccino, G., Stephan, K. M., Rizzolatti, G., Seitz, R. J., & Freund, H.-J. (1999b). A parieto-premotor network for object manipulation: Evidence from neuroimaging. *Experimental Brain Research*, *128*, 210–213.

Binkofski, F., & Buxbaum, L. J. (2013). Two action systems in the human brain. *Brain and Language*, *127*, 222–229.

Borra, E., Belmalih, A., Calzavara, R., Gerbella, M., Murata, A., Rozzi, S., & Luppino, G. (2008). *Cortical connections of the macaque anterior intraparietal (AIP) area. Cerebral Cortex*, *18*.

Borra, E., Ichinohe, N., Sato, T., Tanifuji, M., & Rockland, K. S. (2010). Cortical connections to area TE in monkey: Hybrid modular and distributed organization. *Cerebral Cortex*, *20*, 257–270.

Brodmann, K. (1909). *Vergleichende Lokalisationslehre der Großhirnrinde*. Leipzig: Barth.

Buxbaum, L. J., Veramonti, T., & Schwartz, M. F. (2000). Function and manipulation tool knowledge in apraxia: Knowing "what for" but not "how". *Neurocase*, *6*, 83–97.

Buxbaum, L. J., & Saffran, E. M. (2002). Knowledge of object manipulation and object function: Dissociations in apraxic and nonapraxic subjects. *Brain and Language*, *82*, 179–199.

Cabeza, R., Ciaramelli, E., Olson, I. R., & Moscovitch, M. (2008). The parietal cortex and episodic memory: An attentional account. *Nature Reviews Neuroscience*, *9*, 613–625.

Campanella, F., D'Agostini, S., Skrap, M., & Shallice, T. (2010). Naming manipulable objects: Anatomy of a category specific effect in left temporal tumours. *Neuropsychologia*, *48*, 1583–1597.

Cant, J. S., & Goodale, M. A. (2011). Scratching beneath the surface: New insights into the functional properties of the lateral occipital área and parahippocampal place area. *The Journal of Neuroscience*, *31*, 8248–8258.

Cantlon, J. F. (2013). Math, monkeys, and the developing brain. *Proceedings of the National Academy of the Sciences of the United States of America*, *109*, 10725–10732.

Cantlon, J. F., Libertus, M. E., Pinel, P., Dehaene, S., Brannon, E. M., & Pelphrey, K. P. (2009). The neural development of an abstract concept of number. *Journal of Cognitive Neuroscience*, *21*, 2217–2229.

Capitani, E., Laiacona, M., Mahon, B., & Caramazza, A. (2003). What are the facts of semantic category-specific deficits? A critical review of the clinical evidence. *Cognitive Neuropsychology*, *20*, 213–261.

Caspers, S., Geyer, S., Schleicher, A., Mohlberg, H., Amunts, K., & Zilles, K. (2006). The human inferior parietal cortex: Cytoarchitectonic parcellation and inter-individual variability. *NeuroImage*, *33*, 430–448.

Caspers, S., Eickhoff, S. B., Rick, T., von Kapri, A., Kuhlen, T., Huang, R., Shah, N. J., & Zilles, K. (2011). Probabilistic fibre tract analysis of cytoarchitectonically defined human inferior parietal lobule areas reveals similarities to macaques. *NeuroImage*, *58*, 362–380.

Caspers, S., Schleicher, A., Bacha-Trams, M., Palomero-Gallagher, N., Amunts, K., & Zilles, K. (2013). Organization of human inferior parietal lobule based on receptor architectonics. *Cerebral Cortex*, *53*, 615–628.

Cavina-Pratesi, C., Goodale, M. A., & Culham, J. C. (2007). FMRI Reveals a dissociation between grasping and perceiving the size of real 3D objects. *PLoS One*, *2*, 1–14.

Chao, L. L., Haxby, J. V., & Martin, A. (1999). Attribute-based neural substrates in temporal cortex for perceiving and knowing about object. *Nature Neuroscience*, *2*, 913–919.

Chao, L. L., & Martin, A. (2000). Representation of manipulable man-made objects in the dorsal stream. *Neuroimage*, *12*, 478–484.

Corbetta, M. (1998). Frontoparietal cortical networks for directing attention and the eye to visual locations: Identical, independent, or overlapping neural systems? *Proceedings of the National Academy of the Sciences of the United States of America*, *95*, 831–838.

Corbetta, M., & Shulman, G. L. (2002). Control of goal-directed and stimulus-driven attention in the brain. *Nature Reviews Neuroscience*, *3*, 201–215.

Creem-Regehr, S. H., & Lee, J. N. (2005). Neural representations of graspable objects: Are tools special? *Cognitive Brain Research*, *22*, 457–469.

Cubelli, R., Marchetti, C., Boscolo, G., & Della Salla, S. (2000). Cognition in action: Testing a model of limb apraxia. *Brain and Cognition*, *44*, 144–165.

Culham, J. C., Danckert, S. L., DeSouza, J. F. X., Gati, J. S., Menon, R. S., & Goodale, M. A. (2003). Visually guided grasping produces fMRI activation in dorsal but not ventral brain areas. *Experimental Brain Research*, *153*, 180–189.

Desmurget, M., & Sirigu, A. (2009). A parietal-premotor network for movement intention and motor awareness. *Trends in Cognitive Sciences*, *13*, 411–419.

Durand, J.-B., Nelissen, K., Joly, O., Wardak, C., Todd, J. T., et al. (2007). Anterior regions of monkey parietal cortex process visual 3D shape. *Neuron*, *55*, 493–505.

Fang, F., & He, S. (2005). Cortical responses to invisible objects in the human dorsal and ventral pathways. *Nature Neuroscience*, *8*, 1380–1385.

Gainotti, G. (2000). What the locus of brain lesions tells us about the nature of the cognitive defect underlying category-specific disorders: A review. *Cortex*, *36*, 539–559.

Gainotti, G. (1995). Neuroanatomical correlates of category-specific semantic disorders: A critical survey. *Memory*, *3*, 247–264.

Garcea, F. E., Dombovy, M., & Mahon, B. Z. (2013). Preserved tool knowledge in the context of impaired action knowledge: Implications for models of semantic memory. *Frontiers in Human Neuroscience*, *7*, 1–18.

Geschwind, N. (1965). Disconnexion syndromes in animals and man. Part II. *Brain*, *8*, 585–644.

Goldenberg, G. (2009). Apraxia and the parietal lobes. *Neuropsychology*, *47*, 1449–1459.

Grafton, S. T., Fadiga, L., Arbib, M. A., & Rizzolatti, G. (1997). Premotor cortex activation during observation of familiar tools. *NeuroImage*, *6*, 231–236.

Grill-Spector, K., Henson, R., & Martin, A. (2006). Repetition and the brain: Neural models of stimulus-specific effects. *Trends in Cognitive Science*, *10*, 14–23.

Gotts, S.J., Jo, H.J., Wallace, G.L., Saad, Z.S., Cox, R.W., and Martin, A. (in press). Two distinct forms of functional lateralization in the human brain. Proceedings of the National Academy of the Sciences of the United State of America. http://dx.doi.org/10.1073/pnas.1302581110.

Gotts, S. J., Saad, Z. S., Jo, H. J., Wallace, G. L., Cox, R. W., & Martin, A. (2013). The perils of global signal regression for group comparisons: A case study of Autism Spectrum Disorders. *Frontiers in Human Neuroscience*, *7*, 1–20.

He, B. J., Snyder, A. Z., Vincent, J. L., Epstein, A., Shulman, G. L., & Corbetta, M. (2007). Breakdown of functional connectivity in frontoparietal networks underlies behavioral deficits in spatial neglect. *Neuron*, *53*, 905–918.

Hickok, G. (2009). The functional neuroanatomy of language. *Physics of Life Reviews*, *6*, 121–143.

Hickok, G., & Poeppel, D. (2004). Dorsal and ventral streams: A framework for understanding aspects of the functional anatomy of language. *Cognition*, *92*, 67–99.

Jeannerod, M., Arbib, M. A., Rizzolatti, G., & Sakata, H. (1995). Grasping objects: The cortical mechanisms of visuomotor transformation. *Trends in Neuroscience*, *18*, 314–320.

Jeannerod, M., Decety, J., & Michel, F. (1994). Impairment of grasping movements following a bilateral posterior parietal lesion. *Neuropsychologia*, *32*, 369–380.

Johnson-Frey, S. (2004). The neural bases of complex tool use in humans. *Trends in Cognitive Sciences*, *8*, 71–78.

Johnson-Frey, S., Newman-Norlund, R., & Grafton, S. T. (2005). A distributed left hemipshere network active during planning of everyday tool use skills. *Cerebral Cortex*, *15*, 681–695.

Karnath, H. O., & Perenin, M. T. (2005). Cortical control of visually guided reaching: Evidence from patients with optic ataxia. *Cerebral Cortex*, *15*, 1561–1569.

Konen, C. S., Kleiser, R., Wittsack, H.-J., Bremmer, F., & Seitz, R. J. (2004). The encoding of saccadic eye movements within human posterior parietal cortex. *NeuroImage*, *22*, 304–314.

Konen, C. S., & Kastner, S. (2008). Two hierarchically organized neural systems for object information in human visual cortex. *Nature Neuroscience*, *11*, 224–231.

Konen, C. S., Mruczek, R. E. B., Montoya, J. L., & Kastner, S. (2013). Functional organization of human posterior parietal cortex: Grasping- and reaching-related activations relative to topographically organized cortex. *Journal of Neurophysiology*, *109*, 2897–2908.

Leiguarda, R. C., & Marsden, C. D. (2000). Limb apraxias: Higher-order disorders of sensorimotor integration. *Brain*, *123*, 860–879.

Liepmann, H. (1905). The left hemisphere and action. (Translation from Munch. Med. Wschr. 48–49). (Translations from Liepmann's essays on apraxia. In *Research bulletin* (Vol. 506). London, Ont.: Department of Psychology, University of Western Ontario; 1980).

Lewis, J. (2006). Cortical networks related to human use of tools. *The Neuroscientist*, *12*, 211–231.

Mahon, B. Z., & Caramazza, A. (2005). The orchestration of the sensory-motor systems: Clues from neuropsychology. *Cognitive Neuropsychology*, *22*, 480–494.

Mahon, B. Z., Milleville, S., Negri, G. A. L., Rumiati, R. I., Caramazza, A., & Martin, A. (2007). Action-related properties of objects shape object representations in the ventral stream. *Neuron*, *55*, 507–520.

Mahon, B. Z., Kumar, N., & Almeida, J. (2013). Spatial frequency tuning reveals interactions between the dorsal and ventral visual systems. *Journal of Cognitive Neuroscience*, *25*, 862–871.

Mars, R. B., Jbabdi, S., Sallet, J., O'Reilly, J. X., Croxson, P. L., et al. (2011). Diffusion-weighted imaging tractography-based parcellation of the human parietal cortex and comparison with human and macaque resting-state functional connectivity. *The Journal of Neuroscience*, *31*, 4087–4100.

Martin, A., Wiggs, C. L., Ungerleider, L. G., & Haxby, J. V. (1996). Neural correlates of category-specific knowledge. *Nature*, *379*, 649–653.

Martin, A. (2007). The representation of object concepts in the brain. *Annual Review of Psychology*, *58*, 25–45.

Matelli, M., Luppino, G., & Rizzolatti, G. (1985). Patterns of cytochrome oxidase activity in the frontal agranular cortex of macaque monkey. *Behavioral Brain Research*, *18*, 125–137.

Matelli, M., Luppino, G., & Rizzolatti, G. (1991). Architecture of superior and mesial area 6 and of the adjacent cingulate cortex. *Journal of Comparative Neurology*, *311*, 445–462.

Merigan, W. H., & Maunsell, J. H. (1993). How parallel are the primate visual pathways? *Annual Review of Neuroscience*, *16*, 369–402.

Miceli, G., Fouch, E., Capasso, R., Shelton, J. R., Tomaiuolo, F., & Caramazza, A. (2001). The dissociation of color from form and function knowledge. *Nature Neuroscience*, *4*, 662–667.

Milner, A. D., & Goodale, M. A. (2008). Two visual systems re-viewed. *Neuropsychologia*, *46*, 774–785.

Mirkin, B. (2005). *Clustering for data mining: A data recovery approach*. Boca Raton: Chapman and Hall/CRC.

Negri, G. A. L., Rumiati, R. I., Zadini, A., Ukmar, M., Mahon, B. Z., & Caramazza, A. (2007). What is the role of motor simulation in action and object recognition? Evidence from apraxia. *Cognitive Neuropsychology*, *24*, 795–816.

Nelsen, S. M., Cohen, A. L., Power, J. D., Wig, G. S., Miezin, F. M., et al. (2010). A parcellation scheme for human left lateral parietal cortex. *Neuron*, *67*, 156–170.

Noppeney, U., Price, C. J., Penny, W. D., & Friston, K. J. (2006). Two distinct neural mechanisms for category-selective responses. *Cerebral Cortex*, *16*, 437–445.

Ochipa, C., Rothi, L. J. G., & Heilman, K. M. (1989). Ideational apraxia: A deficit in tool selection and use. *Annals of Neurology*, *25*, 190–193.

Orban, G. A., Claeys, K., Nelissen, K., Smans, R., Sunaert, S., et al. (2006). Mapping the parietal cortex of human and non-human primates. *Neuropsychologia*, *44*, 2647–2667.

Osiurak, F., Jarry, C., & Le Gall, D. (2009). Re-examining the gesture engram hypothesis: New perspectives on apraxia of tool use. *Neuropsychologia*, *49*, 299–312.

Pandya, D. N., & Kuypers, H. G. J. M. (1969). Cortico-cortical connections in the rhesus monkey. *Brain Research*, *13*, 13–36.

Pandya, D. N., & Seltzer, B. (1982). Intrinsic connections and architectonics of posterior parietal cortex in the rhesus monkey. *Journal of Comparative Neurology*, *204*, 196–210.
Passingham, R. E. (1985). Premotor cortex: Sensory cues and movement. *Behavioural Brain Research*, *18*, 175–185.
Pelli, D. G. (1997). The VideoToolbox software for visual psychophysics: Transforming numbers into movies. *Spatial Vision*, *10*, 377–401.
Pisella, L., Gréa, H., Tilikete, C., Vighetto, A., Desmurget, M., et al. (2000). An 'automatic pilot' for the hand in human posterior parietal cortex: Toward reinterpretation of optic ataxia. *Nature Neuroscience*, *3*, 729–736.
Rizzolatti, G., & Matelli, M. (2003). Two different streams form the dorsal visual system: Anatomy and functions. *Experimental Brain Research*, *153*, 146–157.
Rogers, T. T., Hocking, J., Mechelli, A., Patterson, K., & Price, C. (2005). Fusiform activation to animals is driven by the process, not the stimulus. *Journal of Cognitive Neuroscience*, *17*, 434–445.
Rumiati, R. I., Zanini, S., Vorano, L., & Shallice, T. (2001). A form of ideational apraxia as a selective deficit of contention scheduling. *Cognitive Neuropsychology*, *18*, 617–642.
Rumiati, R. I., Weiss, P. H., Shallice, T., Ottoboni, G., Noth, J., Zilles, K., & Fink, G. R. (2004). Neural basis of pantomiming the use of visually presented objects. *NeuroImage*, *21*, 1224–1231.
Rothi, L. J. G., Ochipa, C., & Heilman, K. M. (1991). A cognitive neuropsychological model of limb praxis. *Cognitive Neuropsychology*, *8*, 443–458.
Rozzi, S., Calzavara, R., Belmalih, A., Borra, E., Gregoriou, G. G., Matelli, M., & Luppino, G. (2006). Cortical connections of the inferior parietal cortical convexity of the macaque monkey. *Cerebral Cortex*, *16*, 1389–1417.
Ruschel, M., Knosche, T. R., Friederici, A. D., Turner, R., Geyer, S., and Anwander, A. (in press). Connectivity architecture and subdivision of the human inferior parietal cortex revealed by diffusion MRI. *Cerebral Cortex*, http://dx.doi.org/10.1093/cercor/bht098.
Rushworth, M. F. S., Behrens, T. E. J., & Johansen-Berg, H. (2006). Connection patterns distinguish 3 regions of human parietal cortex. *Cerebral Cortex*, *16*, 1418–1430.
Saad, Z. S., Reynolds, R. C., Jo, H. J., Gotts, S. J., Chen, G., Martin, A., & Cox, R. W. (2013). Correcting brain-wide correlation differences in resting-state fMRI. *Brain Connectivity,*, *3*, 339–352.
Schwarzbach, J. (2011). A simple framework (ASF) for behavioral and neuroimaging experiments based on psychophysics toolbox for MATLAB. *Behavioral Research*, *43*, 1194–1201.
Talairach, J., & Tournoux, P. (1988). *Co-planar stereotaxic atlas of the human brain*. New York: Thieme.
Thiebaut de Schotten, M., Urbanski, M., Duffau, H., Volle, E., Lévy, R., Dubois, B., & Bartolomeo, P. (2005). Direct evidence for a parietal-frontal pathway subserving spatial awareness in humans. *Science*, *309*, 2226–2228.
Thiebaut de Schotten, M., Dell'Acqua, F., Forkel, S. J., Simmons, A., Vergani, F., et al. (2011). A lateralized brain network for visuospatial attention. *Nature Neuroscience*, *14*, 1245–1246.
Vogt, C., & Vogt, O. (1919). Ergebnisse unserer Hirnforschung. Vierte mitteilung: Die physiologische bedeutung der architektonischen rin-denreizungen. *Journal f. Psychologie und Neurologie*, *25*, 279–461.
von Economo, C. (1929). *The cytoarchitectonics of the human cerebral cortex*. London: Oxford University Press (186 pp).
von Economo, K., & Koskinas, G. (1925). *Die Cytoarchitektonik der Hirnrinde des erwachsenen Menschen*. Wien: Springer.
Zhang, Y., Fan, L., Zhang, Y., Wang, J., Zhu, M., et al. (2014). Connectivity-based parcellation of the human posteromedial cortex. *Cerebral Cortex,*, *24*, 719–727.
Zhong, Y., & Rockland, K. S. (2003). Inferior parietal lobule projections to anterior inferotemporal cortex (Area TE) in macaque monkey. *Cerebral Cortex*, *13*, 527–540.